Pseudopotential of hybrid mesons in a holographic anisotropic plasma*

Jing Zhou (周京)[1,2†] Saiwen Zhang (张赛文)[1,2]

[1]Department of Physics, Hunan City University, Yiyang, Hunan 413000, China
[2]All-solid-state Energy Storage Materials and Devices Key Laboratory of Hunan Province, Hunan City University, Yiyang 413000, China

Abstract: We investigate the pseudopotential of hybrid mesons in a holographic anisotropic background within the AdS/CFT correspondence. Hybrid states are modeled by introducing a defect, and we analyze the associated force-balance condition in the string configuration. From this setup, we derive the balance equation and compute key physical quantities, including the separation distance, pseudopotential, and binding energy of the hybrid mesons. We find that increasing the anisotropy parameter a decreases the separation distance for both ground and excited states. However, while the ground-state potential decreases, the pseudopotential of the hybrid state increases. Additionally, the pseudopotential of hybrid mesons exhibits significant sensitivity to variations in the angular parameter α.

Keywords: pseudopotential, hybrid mesons, anisotropy parameter

DOI: 10.1088/1674-1137/ae5a88 **CSTR:** 32044.14.ChinesePhysicsC.50063108

I. INTRODUCTION

The quark-antiquark potential plays a fundamental role in understanding the interaction between a quark and an antiquark [1, 2]. Its study is essential not only for describing the formation of heavy quarkonia but also for exploring the properties of the quark-gluon plasma (QGP) [3−5]. It is generally understood that the static quark-antiquark potential consists of two main contributions: a short-distance Coulomb-like term, which can be derived from perturbative QCD, and a long-distance linear potential associated with confinement [6−10]. The interaction potential between quarks and antiquarks is commonly evaluated by calculating Wilson loop expectation values within the non-perturbative regime of lattice QCD [11−18]. Effective field theory approaches, such as potential non-relativistic QCD (pNRQCD), offer an alternative perspective by systematically incorporating the relevant energy scales [19−23]. However, both approaches have limitations. For example, lattice QCD calculations are performed in Euclidean time and therefore do not provide direct access to real-time transport coefficients [24]. These quantities must be extracted indirectly through the reconstruction of spectral functions, a numerically challenging inverse problem. By contrast, perturbative QCD is restricted to the weak-coupling regime and cannot capture the strongly coupled nature or the infrared physics of the QGP. Given these challenges, the AdS/CFT correspondence offers an alternative approach by mapping the problem of strong coupling in gauge theory to a weakly coupled classical gravity description in a higher-dimensional spacetime [25−29]. This duality provides a theoretical framework for investigating non-perturbative phenomena, thereby allowing the computation of the quark-antiquark potential under strong-coupling conditions.

Ref. [30] applies the AdS/CFT correspondence to compute the static quark-antiquark potential using the Wilson loop. This approach extends to the study of both the static potential and the pseudopotential under various conditions. The static potential corresponds to the ground-state energy of the quark-antiquark pair, whereas the pseudopotential describes the energy of an excited state. For instance, Ref. [31] examines the quark-antiquark potential in a background magnetic field and finds that increasing the field strength reduces the potential. In a rotating background, the potential also decreases as the angular velocity increases [32]. Other studies explore the potential under various extreme conditions, thereby providing further insights into quark confinement and screening effects [33−49].

Hybrid mesons differ from conventional mesons in that the flux tube connecting the quark and antiquark carries gluonic excitations [50]. These excitations modify the meson spectrum and permit quantum numbers that are forbidden to ordinary states. Studying hybrid mesons elucidates the behavior of the gluonic sector in hadronic dynamics. Allowed decay patterns have been investigated via lattice QCD in Ref. [51], and the impact of these

Received 23 September 2025; Accepted 26 March 2026; Accepted manuscript online 27 March 2026

* Supported in part by the Natural Science Foundation of Hunan Province, China (2024JJ6108) and the Scientific Research Fund of the Hunan Provincial Education Department (23A0571)

† E-mail: zhoujing@hncu.edu.cn

gluonic excitations on the mass spectrum has been systematically mapped out in Ref. [52], particularly within a quenched QCD framework. A study of light-quarkonium hybrid mesons with various spin-parity quantum numbers is presented in Ref. [53]. Further studies of hybrid mesons, covering different aspects of their properties, can be found in Refs. [54−63].

Recently, following the proposal of Andreev *et al*., holographic approaches have been employed to study quark-antiquark potentials and pseudopotentials within the framework of ten-dimensional string theory [64, 65]. Unlike the static $Q\bar{Q}$ and QQQ potentials analyzed in Ref. [66], determining the pseudopotential for hybrid mesons requires introducing a defect. The contribution of this defect can be effectively captured by the action of a five-dimensional brane, which in turn enables a description of the gluon field in an excited state. The defect is assumed to be embedded in the ten-dimensional string spacetime [67]. In their study, Andreev *et al*. examined the pseudopotential for the excited Σ meson and the static potential for the ground-state Σ meson [67]. Their results align well with lattice QCD calculations, thereby demonstrating the reliability of this model.

However, to the best of our knowledge, the quark-antiquark pseudopotential for hybrid mesons in an anisotropic background has not yet been explored. Initial-state geometric asymmetry in relativistic heavy-ion collisions naturally gives rise to non-uniform pressure gradients as the system undergoes hydrodynamic expansion. Previous studies indicate that the physics in anisotropic backgrounds differs markedly from that in isotropic systems. Motivated by these considerations, we investigate the pseudopotential for hybrid mesons within a ten-dimensional anisotropic string model. In Sec. II, we introduce the ten-dimensional model, explain the rationale for including defects, and show how to compute their contribution to the hybrid-meson pseudopotential. This sets the foundation for deriving the hybrid-meson separation distance and pseudopotential, which are discussed in detail. Sec. III presents a comparative analysis of the standard quark-antiquark potential and the hybrid-meson pseudopotential. Finally, in Sec. IV we summarize our results and discuss their physical implications within this anisotropic framework.

II. THEORETICAL COMPUTATION OF HYBRID MESON PSEUDOPOTENTIALS

In this section, we briefly outline the string configuration used to describe excited quark–antiquark pairs. In the ground-state configuration, the quark pair is connected by a fundamental string with a smooth, U-shaped geometry. For excited states, however, it is necessary to introduce an additional object—referred to as a defect—which captures the excitation of the color flux tube. Physically, this defect represents excited gluonic fields between the quark and antiquark. As a result, the string profile in the excited configuration develops a cusp at the defect, rendering the solution non-smooth, as illustrated in Fig. 1 [68]. In this setup, the quark and antiquark are symmetrically located on opposite sides of the u-axis, with the fundamental strings extending from these endpoints toward a common defect situated on the u-axis. Consequently, string 1 makes a nonzero angle α with respect to the x-axis, in contrast to the ground-state configuration, where this angle vanishes.

The present study investigates the behavior of excited mesons in the presence of anisotropy. The anisotropy arises from a finite-temperature deformation of $\mathcal{N}=4$ SYM, whose gravity dual is obtained by including the backreaction of D7-branes. These branes induce a nontrivial profile for the axion field χ along one spatial direction, explicitly breaking rotational invariance. This setup is holographically dual to a gauge theory with a spatially varying θ-term [69]. The corresponding five-dimensional gravity action in the Einstein frame is given by

$$S=\frac{1}{2\kappa^2}\int \mathrm{d}^5x\sqrt{-g}\left[R+12-\frac{1}{2}(\partial\phi)^2-\frac{1}{2}\mathrm{e}^{2\phi}(\partial\chi)^2\right]+S_{\mathrm{GH}}, \tag{1}$$

where R is the Ricci scalar, κ^2 the gravitational coupling, and ϕ the dilaton. The constant term 12 corresponds to setting the AdS radius to unity ($L=1$). This action arises from a consistent truncation of Type IIB supergravity on S^5, where S_{GH} denotes the Gibbons-Hawking boundary

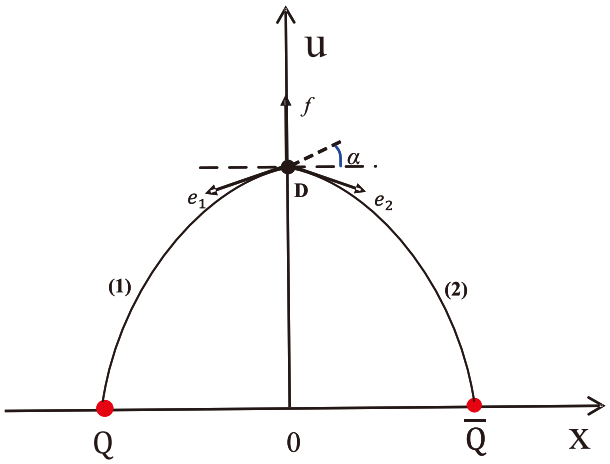

Fig. 1. (color online) Geometric setup of the hybrid meson model [68]. The quark and antiquark are shown as red markers along the x-axis, whereas the holographic defect is represented by a black symbol on the u-axis. The black lines connecting the defect to the quarks represent fundamental strings. The quantities e_1 and e_2 denote the tensions of strings (1) and (2), respectively. The angle between string (1) and the x-axis is denoted by α.

term. The Einstein-frame metric takes the form [69–71]

$$\mathrm{d}s^2 = \frac{1}{u^2}\left(-\mathcal{F}\mathcal{B}\mathrm{d}t^2 + \mathcal{H}\mathrm{d}x^2 + \mathrm{d}y^2 + \mathrm{d}z^2 + \frac{\mathrm{d}u^2}{\mathcal{F}}\right) + \mathcal{Z}\mathrm{d}\Omega_{S^5}^2, \tag{2}$$

$$\chi = a\,x, \quad \phi = \phi(u). \tag{3}$$

Regarding the internal geometry, the factor $\mathcal{Z}(u)$ rescales the internal five-sphere, S^5, whose unit metric is denoted by $\mathrm{d}\Omega_{S^5}^2$. The anisotropy of the dual 4D plasma is introduced via the axion field $\chi = ax$ in the 5D gravity action. Physically, the parameter a corresponds to the constant axion gradient. Through holographic renormalization of the stress-energy tensor $\langle T_{\mu\nu}\rangle$, Ref. [69] established that this setup leads to pressure anisotropy, with the transverse pressure P_T and the longitudinal pressure P_L related by $\Delta = \frac{P_T}{P_L} - 1$. In the limit of small a/T, this relation becomes $\Delta = \frac{a^2}{2\pi^2 T^2}$ [72]. The metric functions can be expanded perturbatively in powers of a. For the anisotropic setup, the metric components $\mathcal{F}(u)$, $\mathcal{B}(u)$, and $\mathcal{H}(u)$ take the following forms [69–71]:

$$\mathcal{F}(u) = 1 - \frac{u^4}{u_h^4} + a^2\mathcal{F}_2(u) + \mathcal{O}\left(a^4\right), \tag{4}$$

$$\mathcal{B}(u) = 1 + a^2\mathcal{B}_2(u) + \mathcal{O}\left(a^4\right), \tag{5}$$

$$\mathcal{H}(u) = \mathrm{e}^{-\phi(u)}, \quad \text{with} \quad \phi(u) = a^2\phi_2(u). \tag{6}$$

Although the analytic expressions are derived for small a/T, we have verified their accuracy by comparison with fully numerical solutions of the governing equations. It has been demonstrated that the saddle-point approximation for the Nambu-Goto action remains robust and accurate for anisotropies as large as $a/T \approx 12$ [72]. Our largest value ($a/T \approx 7$ at $T = 0.1$ GeV) lies well within this numerically verified bound. The second-order coefficients are determined by boundary conditions at the horizon.

$$\mathcal{F}_2(u) = \frac{1}{24u_h^2}\left[8u^2\left(u_h^2 - u^2\right) - 10u^4\log 2 + \left(3u_h^4 + 7u^4\right)\log\left(1 + \frac{u^2}{u_h^2}\right)\right], \tag{7}$$

$$B_2(u) = -\frac{u_h^2}{24}\left[\frac{10u^2}{u_h^2 + u^2} + \log\left(1 + \frac{u^2}{u_h^2}\right)\right], \tag{8}$$

$$\phi_2(u) = -\frac{u_h^2}{4}\log\left(1 + \frac{u^2}{u_h^2}\right). \tag{9}$$

Thus the temperature is given by

$$T = -\left.\frac{\partial_u\mathcal{F}(u)\sqrt{\mathcal{B}(u)}}{4\pi}\right|_{u=u_h} = \frac{1}{\pi u_h} + a^2 u_h\frac{5\log 2 - 2}{48\pi} + \mathcal{O}\left(a^4\right). \tag{10}$$

The plasma considered in this work is homogeneous yet anisotropic. While translational invariance is preserved, rotational symmetry is explicitly broken by the axion field. Consequently, the temperature, set by the Hawking temperature of the black brane, is uniform and independent of the spatial coordinate x.

Following Ref. [67], we construct the total action for the pseudopotential of the excited meson by combining the Nambu-Goto term with an additional contribution due to the defect:

$$S = \sum_{i=1}^{2} S_i^{(\mathrm{NG})} + S_{\mathrm{def}}, \tag{11}$$

where $S_i^{(\mathrm{NG})}$ denotes the Nambu-Goto action of the i-th string segment that stretches from a heavy quark (or antiquark) on the boundary to a defect in the bulk. The two string segments reflect the hybrid meson configuration, in which the quark and antiquark are connected by an intermediate gluonic excitation. In the static limit, we describe the string trajectory via the embedding $u = u(x)$ with the gauge choice $\tau = t$ and $\sigma = x$. The corresponding Nambu-Goto action for each string segment is given by

$$S^{\mathrm{NG}} = \frac{1}{2\pi\alpha'}\int \mathrm{d}\tau\mathrm{d}\sigma\,\sqrt{-\det g_{ab}}, \tag{12}$$

Here, g_{ab} denotes the worldsheet metric induced from the bulk spacetime metric $G_{\mu\nu}$ via $g_{ab} = G_{\mu\nu}\partial_a X^\mu \partial_b X^\nu$.

The main difficulty lies in determining the defect contribution. Following the holographic framework of Ref. [67], the defect is modeled as a fivebrane-antifivebrane pair embedded in a ten-dimensional background. The leading-order dynamics of these fivebranes are governed by the Dirac-Born-Infeld (DBI) action, which is proportional to the world-volume of the branes, $S_{\mathrm{def}} \sim \int \mathrm{d}^6\xi\,\sqrt{-g_6}$, where g_6 is the induced metric [67]. By evaluating the induced metric g_6 in the string frame and integrating over the compact dimensions, one finds that the action for this configuration reduces to an effective contribution localized at the turning point u_0 [67, 73]:

$$S_{\rm def} = \int {\rm d}t \sqrt{\frac{\mathcal{F}(u_0)\mathcal{B}(u_0){\rm e}^{\frac{5}{2}\phi}}{u_0^2}}. \tag{13}$$

Consequently, the complete holographic action is given by:

$$\begin{aligned} S =& 2g\mathcal{T}\int {\rm d}x \frac{\sqrt{\mathcal{B}(u)}}{u^2}\sqrt{\mathcal{F}(u)\mathcal{H}(u)+(\partial_x u)^2} \\ &+2\,{\rm k}g\mathcal{T}\sqrt{\frac{\mathcal{F}(u_0)\mathcal{B}(u_0){\rm e}^{\frac{5}{2}\phi}}{u_0^2}}. \end{aligned} \tag{14}$$

Here, g and k are phenomenological parameters that characterize the strength of the gluonic defect contribution in the hybrid configuration. Consistent with Refs. [67, 73], we set $g = 0.176$. $\mathcal{T}$ denotes the temporal extent of the Wilson loop. Following the structure of Eq. (14), the Lagrangian for the first part is given by:

$$\mathcal{L} = \frac{\sqrt{\mathcal{B}(u)}}{u^2}\sqrt{\mathcal{F}(u)\mathcal{H}(u)+(\partial_x u)^2}. \tag{15}$$

Given that the Lagrangian does not explicitly depend on the coordinate x, the Hamiltonian-like quantity $\mathcal{L}-u'\dfrac{\partial\mathcal{L}}{\partial u'}$ serves as a first integral of the equations of motion. By evaluating this conserved current C at the defect junction **D** (located at $u=u_0$) and imposing the geometric condition $\partial_x u = \tan\alpha$, we find that, at the defect **D** located at u_0, we have [71]

$$\frac{\frac{\sqrt{\mathcal{B}(u)}}{u^2}\mathcal{F}(u)\mathcal{H}(u)}{\sqrt{\mathcal{F}(u)\mathcal{H}(u)+(\partial_x u)^2}} = \frac{\sqrt{\mathcal{B}(u_0)}}{u_0^2}\sqrt{\mathcal{F}(u_0)\mathcal{H}(u_0)}. \tag{16}$$

After applying this matching procedure and rearranging the terms to isolate the spatial gradient, we obtain the following relation for the trajectory of the holographic string:

$$\partial_u x = \sqrt{\frac{\frac{\mathcal{B}(u_0)}{u_0^4}\mathcal{F}^2(u_0)\mathcal{H}^2(u_0)}{\frac{\mathcal{B}(u)}{u^4}\mathcal{F}^2(u)\mathcal{H}^2(u)\mathcal{F}(u_0)\mathcal{H}(u_0)-\frac{\mathcal{B}(u_0)}{u_0^4}\mathcal{F}^2(u_0)\mathcal{H}^2(u_0)\mathcal{F}(u)\mathcal{H}(u)}}. \tag{17}$$

The mechanical stability of the junction is governed by the force-balance equation $\boldsymbol{e}_1+\boldsymbol{e}_2+\boldsymbol{f}=0$, as depicted in Fig. 1. Here, $\boldsymbol{e}_i$ denote the string tensions, and $\boldsymbol{f}$ accounts for the gravitational effect at the defect, which is defined via the variation $\boldsymbol{f} = -\delta E_{\rm def}/\delta u$. Due to transverse symmetry in the x-direction, we only need to consider equilibrium in the holographic direction. Therefore, each force and its components are given by [68]

$$\begin{aligned} \boldsymbol{f} =& \left(0, -2g{\rm k}\partial_{u_0}\sqrt{\frac{\mathcal{F}(u_0)\mathcal{B}(u_0){\rm e}^{\frac{5}{2}\phi}}{u^2}}\right), \\ \boldsymbol{e_1} =& g\frac{\sqrt{\mathcal{B}(u_0)}}{u_0^2}\left(-\frac{\mathcal{F}(u_0)\mathcal{H}(u_0)}{\sqrt{\mathcal{F}(u_0)\mathcal{H}(u_0)+\tan^2\alpha}},\right. \\ &\left.-\frac{1}{\sqrt{1+\mathcal{F}(u_0)\mathcal{H}(u_0)\cot^2\alpha}}\right), \\ \boldsymbol{e}_2 =& g\frac{\sqrt{\mathcal{B}(u_0)}}{u_0^2}\left(\frac{\mathcal{F}(u_0)\mathcal{H}(u_0)}{\sqrt{\mathcal{F}(u_0)\mathcal{H}(u_0)+\tan^2\alpha}},\right. \\ &\left.-\frac{1}{\sqrt{1+\mathcal{F}(u_0)\mathcal{H}(u_0)\cot^2\alpha}}\right). \end{aligned} \tag{18}$$

By symmetry, the transverse components of the force in the x-y plane cancel identically. Accordingly, the condition of mechanical equilibrium reduces to the following transcendental equation for u_0:

$$\frac{\sqrt{\mathcal{B}(u_0)}}{u_0^2}\frac{1}{\sqrt{1+\mathcal{F}(u)\mathcal{H}(u)\cot^2\alpha}}+k\partial_{u_0}\sqrt{\frac{\mathcal{F}(u_0)\mathcal{B}(u_0){\rm e}^{\frac{5}{2}\phi}}{u_0^2}}=0. \tag{19}$$

Solving Eq. (19) yields u_0 directly. The separation distance can be computed by integrating Eq. (17) as follows [66, 74]:

$$\begin{aligned} L =& \int_0^{u_0}\frac{{\rm d}x}{{\rm d}u}{\rm d}u \\ =& \int_0^{u_0}\sqrt{\frac{\frac{\mathcal{B}(u_0)}{u_0^4}\mathcal{F}^2(u_0)\mathcal{H}^2(u_0)}{\frac{\mathcal{B}(u)}{u^4}\mathcal{F}^2(u)\mathcal{H}^2(u)\mathcal{F}(u_0)\mathcal{H}(u_0)-\frac{\mathcal{B}(u_0)}{u_0^4}\mathcal{F}^2(u_0)\mathcal{H}^2(u_0)\mathcal{F}(u)\mathcal{H}(u)}}{\rm d}u. \end{aligned} \tag{20}$$

When $\partial_x u = \tan\alpha = 0$, the equation reduces to the one

used to compute the separation distance of a standard quark-antiquark pair. Within the AdS/CFT correspondence, the static energy of a quark-antiquark configuration is related to the on-shell classical action through the relation $E = S/\mathcal{T}$, where S denotes the total action evaluated on the string configuration. To obtain a finite potential energy for the hybrid meson, the Nambu-Goto action must be regularized by subtracting the ultraviolet (UV) divergence. This is typically achieved by removing the self-energy contribution of the bare quarks, which corresponds to the term $g\int_0^{\infty}\frac{1}{u^2}\mathrm{d}u$. Consequently, the renormalized potential energy is given by [71]:

$$E = 2g\int_0^{u_0}\left(\frac{\sqrt{\mathcal{B}(u)}}{u^2}\sqrt{1+\mathcal{F}(u)\mathcal{H}(u)(\partial_u x)^2}-\frac{1}{u^2}\right)\mathrm{d}u - \frac{2g}{u_0}+2g\mathrm{k}\sqrt{\frac{\mathcal{F}(u_0)\mathcal{B}(u_0)\mathrm{e}^{\frac{5}{2}\phi}}{u_0^2}}+c. \tag{21}$$

In accordance with Refs. [67, 73], the model parameter is taken to be $c = 0.71\,\mathrm{GeV}$. Following the definition of the binding energy in Refs. [38, 75, 71], the binding energy of the quark-antiquark pair is given by

$$\begin{aligned} E_{bind} &= E - 2E_Q \\ &= 2g\int_0^{u_0}\left(\frac{\sqrt{\mathcal{B}(u)}}{u^2}\sqrt{1+\mathcal{F}(u)\mathcal{H}(u)(\partial_u x)^2}-\frac{1}{u^2}\right)\mathrm{d}u \\ &\quad -\frac{2g}{u_0}+2g\mathrm{k}\sqrt{\frac{\mathcal{F}(u_0)\mathcal{B}(u_0)\mathrm{e}^{\frac{5}{2}\phi}}{u_0^2}}+c \\ &\quad -g\left(\int_0^{u_h}\left(\frac{\sqrt{\mathcal{B}(u)}}{u^2}\sqrt{\mathcal{F}(u)\mathcal{H}(u)}-\frac{1}{u^2}\right)\mathrm{d}u-\frac{1}{u_h}\right). \end{aligned} \tag{22}$$

The self-contribution E_Q of a single quark is given by the action of a vertical string segment connecting the UV boundary ($u = 0$) to the black hole horizon ($u = u_h$). After implementing UV regularization to obtain a finite physical energy [38], one obtains:

$$E_Q = \frac{1}{2}\left(\int_0^{u_h}\left(\frac{\sqrt{\mathcal{B}(u)}}{u^2}\sqrt{\mathcal{F}(u)\mathcal{H}(u)}-\frac{1}{u^2}\right)\mathrm{d}u-\frac{1}{u_h}\right). \tag{23}$$

III. NUMERICAL ANALYSIS

Building on the theoretical formalism introduced in the previous section, we investigate the behavior of exotic hybrid pseudopotentials in anisotropic backgrounds. Unlike conventional heavy-quarkonium systems, exotic hybrid mesons incorporate a topological defect **D**. We first quantify the dependence of the angular parameter α on the defect coordinate u_0, as shown in Fig. 2. The numerical results indicate a monotonic increase of α with increasing u_0, consistent with the geometric configuration in Fig. 1. As u_0 increases, the angular separation between the principal axes $e_1(e_2)$ and the X-axis, which defines α, increases accordingly. The presence of the defect **D** motivates a detailed analysis of its mechanical response. As shown in Fig. 3, we examine the dependence of the force acting on this defect on the parameter u_0. The results reveal a clear trend: the force magnitude diverges at small u_0 and asymptotically approaches zero as u_0 increases.

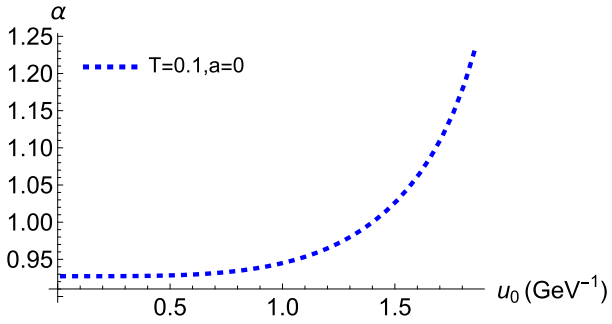

Fig. 2. (color online) Angular profile α as a function of the bulk turning point u_0 for the isotropic case ($a = 0$), evaluated at the thermal scale $T = 0.1\,\mathrm{GeV}$.

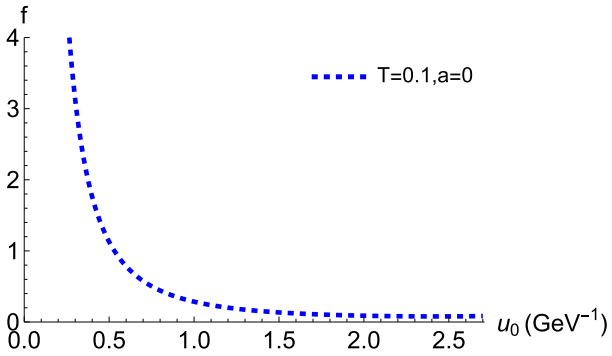

Fig. 3. (color online) Numerical dependence of f on the bulk turning point u_0 in the isotropic case ($a = 0$) at $T = 0.1\,\mathrm{GeV}$.

The maximum screening distance is the greatest separation at which a quark-antiquark pair can remain bound; beyond this distance, the pair becomes unstable due to the medium screening effects, ultimately leading to dissociation. In Fig. 4, we calculated the separation distances of Σ_g^+ and Σ_u^- as functions of the anisotropy parameter a at fixed temperatures. The results show that: (1) As a increases, the maximum screening distances of both Σ_g^+ and Σ_u^- decrease monotonically. This indicates that the presence of anisotropy weakens the binding force between quark-antiquark pairs, making them more prone to dissociation. (2) Under identical conditions ($T = 0.1\,\mathrm{GeV}$ and the same a), the maximum separation distance of Σ_u^- is significantly smaller than that of Σ_g^+. For

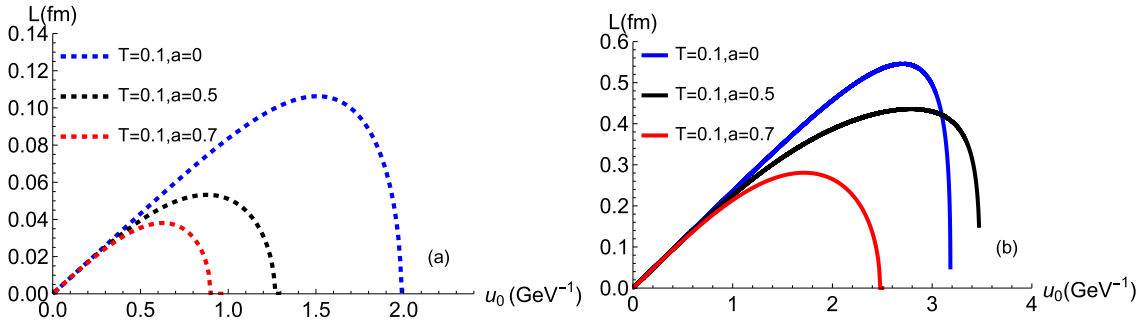

Fig. 4. (color online) Dependence of the separation distance on u_0 for the Σ_g^+ and Σ_u^- channels at $T = 0.1$ GeV and for different values of the anisotropy parameter a. (a) Σ_u^-: Dashed blue, black, and red curves correspond to anisotropy parameters $a = 0$, 0.5, and 0.7, respectively. (b) Σ_g^+: Solid blue, black, and red curves correspond to anisotropy parameters $a = 0$, 0.5, and 0.7, respectively.

example, at $T = 0.1$ GeV and $a = 0.1$, the maximum separation distance of Σ_u^- is approximately 0.04 fm, while that of Σ_g^+ is approximately 0.25 fm. This shows that Σ_u^- dissociates more easily than Σ_g^+ under the same conditions.

Our results indicate that hybrid mesons are more sensitive to anisotropy than ground-state quarkonia. This stems from the excited color flux tube in hybrid states, modeled holographically as a worldsheet defect. The stability of this defect rests on a delicate balance between string tension and background geometry. Anisotropy raises the energy cost of maintaining this excited configuration, disrupting the equilibrium and triggering an earlier onset of instability relative to the ground state.

In Fig. 5, we present a detailed analysis of the dependence of the pseudopotentials in the Σ_g^+ and Σ_u^- channels on the quark-antiquark separation distance L. The results reveal the following characteristics: (1) In the short-distance regime, the pseudopotential in the Σ_g^+ channel exhibits Coulomb-like behavior. Furthermore, as the anisotropy parameter a increases, the magnitude of this pseudopotential decreases monotonically. (2) In contrast, the pseudopotential in the Σ_u^- channel deviates significantly from a Coulomb-like form and is well described by a quadratic dependence on L. This behavior can be attributed to the presence of flux-tube excitations, where the color field configuration corresponds to higher vibrational modes of the gluonic field. In this regime, the energy stored in the flux tube behaves analogously to that of a harmonic oscillator, naturally leading to a quadratic potential profile with respect to the interquark separation. Additionally, this pseudopotential increases with the separation distance and grows larger as the anisotropy parameter a increases.

The hybrid meson potential exhibits a characteristic L^2 dependence, driven by the restoring force of the gluonic defect. In an anisotropic medium, the background geometry alters the effective string tension and thus the stiffness of this force. This modification causes the quadratic growth to collapse earlier than in the isotropic limit, explaining why hybrid mesons show higher sensitivity to anisotropy than ground-state quarkonia.

In the previous discussion, we examined how the pseudopotential characterizes the excited state. However, the binding energy plays a more crucial role in determining whether the excited state can form a stable bound state or remains in an unstable configuration. Specifically, when the binding energy is negative, the excited state is stable and can form a bound state, whereas a positive binding energy indicates that the state cannot bind and is likely to dissociate. In Fig. 6, we show how the

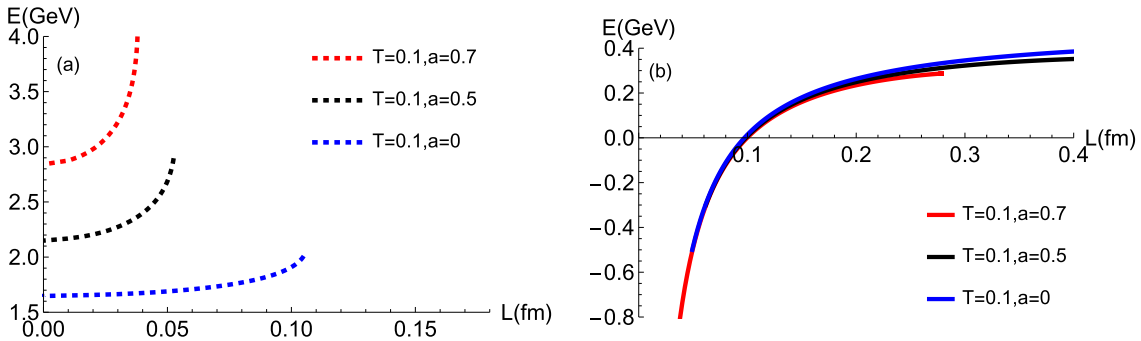

Fig. 5. (color online) Behavior of the static potential for the Σ_u^- (a) and Σ_g^+ (b) channels as a function of the separation L at $T = 0.1$ GeV. (a) In the Σ_u^- channel, the dashed curves correspond to anisotropy parameters $a = 0$ (blue), 0.5 (black), and 0.7 (red). (b) In the Σ_g^+ channel, the solid curves follow the same color scheme for the corresponding a values.

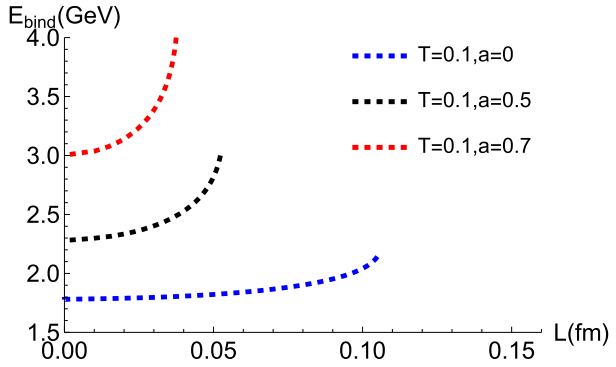

Fig. 6. (color online) Evolution of the binding energy of the Σ_u^- state as a function of the separation L at $T = 0.1\,\mathrm{GeV}$. Dashed blue, black, and red curves represent anisotropy values $a = 0$, 0.5, and 0.7, respectively.

binding energy evolves with the anisotropy parameter a. As a increases, the binding energy in the Σ_u^- channel remains positive and grows larger, which suggests that the corresponding excited state becomes progressively more unstable and increasingly prone to dissociation. The fact that the binding energy of the Σ_u^- hybrid state is consistently positive in Fig. 6 implies that, within the explored temperature and anisotropy range, this hybrid state does not form a stable bound configuration. Physically, this behavior is expected, since hybrid mesons involve explicit gluonic excitations that are more sensitive to color screening effects in a hot and anisotropic plasma. Consequently, such states tend to dissociate more readily than conventional quark-antiquark bound states.

The separation distance of the Σ_u^- state is shown in Fig. 4. Its temperature dependence for fixed anisotropy $a = 0.5$ is further illustrated in Fig. 7. We observe that the maximum separation distance $L_{\max}$ decreases from about 0.055 to 0.045 fm as the temperature increases. This indicates that higher temperatures promote the dissolution of the Σ_u^- state, consistent with Ref. [73]. In Fig. 8, we investigate the temperature dependence of the potential energy of the Σ_u^- state. In our numerical analysis, we focus on $T = 0.10$, 0.15, and 0.16 GeV, values that lie near the QCD deconfinement crossover. In this range, color screening becomes significant and strongly impacts the stability of heavy-quark bound states. The results show that, with increasing temperature, the pseudopotential of Σ_u^- remains positive and gradually increases. This implies that the Σ_u^- excited state becomes increasingly unstable and more susceptible to thermal excitation, leading to dissociation. In the quark model, a key difference between Σ_g^+ and Σ_u^- is the presence of the angle α in the Σ_u^- state, whereas $\alpha = 0$ for Σ_g^+ (see Fig. 1). Accordingly, Fig. 9 examines how the separation distance L varies with α for Σ_u^-. We find that L is not monotonic in α: it increases to a maximum and then gradually decreases, indicating a nonlinear relationship between L and α. We

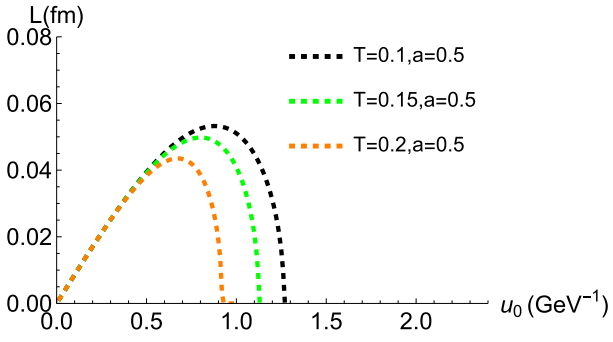

Fig. 7. (color online) Separation distance L as a function of the bulk turning point u_0 ($a = 0.5$). The black, green, and orange dashed lines correspond to thermal scales of 0.1, 0.15, and 0.2 GeV, respectively.

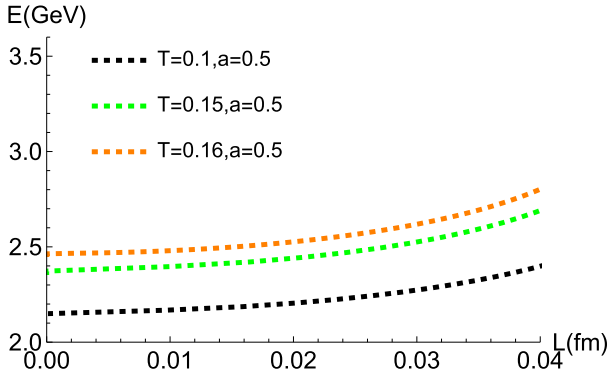

Fig. 8. (color online) The potential energy E of the Σ_u^- state as a function of L for $a = 0.5$. The curves represent temperatures of 0.1 GeV (black dashed), 0.15 GeV (green dashed), and 0.16 GeV (orange dashed).

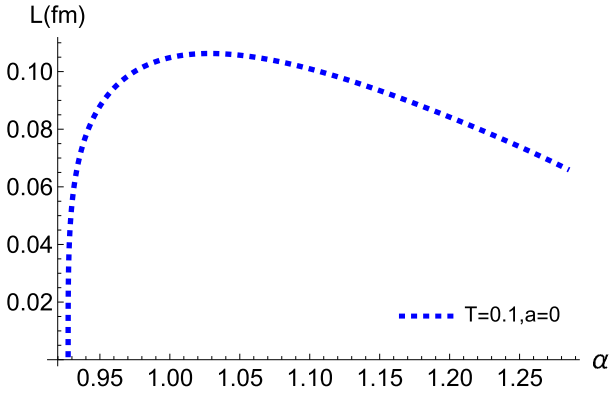

Fig. 9. (color online) The separation distance L as a function of anisotropy a for the Σ_u^- state at $T = 0.1\,\mathrm{GeV}$.

next analyze the effect of α on the Σ_u^- pseudopotential in Fig. 10. As α increases, the pseudopotential falls rapidly from about 25 GeV to roughly 3 GeV, approximately following an exponential decay, demonstrating strong sensitivity to α.

IV. SUMMARY AND CONCLUSIONS

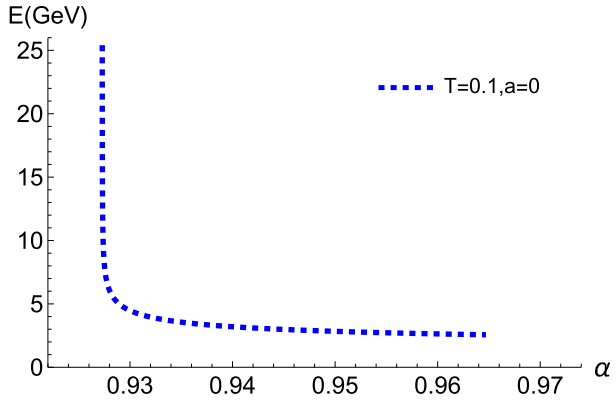

Fig. 10. (color online) Potential energy E as a function of separation L for the Σ_u^- state at $T = 0.1\,\mathrm{GeV}$.

We study the excited-state pseudopotentials for quark-antiquark systems in an anisotropic background. Unlike the ground state, the excited configuration requires the introduction of a defect point **D**. The angle α at this point is fixed by a force-balance condition and increases as the defect is placed deeper in the bulk geometry. The excited-state separation length is then obtained using the same formalism as for the ground state. Our results show that increasing the anisotropy parameter a reduces the maximal separation length in both ground and excited channels, suggesting that anisotropy enhances color-force screening and promotes quark-antiquark dissociation. At short distances, the excited-state pseudopotential deviates from the Coulombic behavior of the ground state, instead scaling quadratically with the interquark distance. This feature reflects the nature of the excited flux tube, consistent with a vibrating system endowed with an effective restoring force. We also analyze the temperature dependence: as the temperature rises, the maximal separation length decreases while the pseudopotential increases, consistent with stronger thermal screening. Finally, we examine the dependence on the angle α: the pseudopotential decreases rapidly with increasing α, exhibiting an approximately exponential decay. This strong sensitivity to geometric deformation highlights the nontrivial structure of the excited configuration.

While this work focuses on mesonic excitations, similar methods can be applied to more complex systems, such as triply heavy baryons. Extending this analysis to excited baryonic configurations in anisotropic media remains an open and interesting direction for future work.

References

[1] T. Matsui and H. Satz, Phys. Lett. B **178**, 416 (1986)
[2] N. Brambilla, S. Eidelman, B. K. Heltsley *et al.*, Eur. Phys. J. C **71**, 1534 (2011), arXiv: 1010.5827[hep-ph]
[3] L. Apolinário, Y. J. Lee, and M. Winn, Prog. Part. Nucl. Phys. **127**, 103990 (2022), arXiv: 2203.16352[hep-ph]
[4] C. Y. Wong, Phys. Rev. C **72**, 034906 (2005), arXiv: 0408020[hep-ph]
[5] A. Mocsy, P. Petreczky, and M. Strickland, Int. J. Mod. Phys. A **28**, 1340012 (2013), arXiv: 1302.2180[hep-ph]
[6] O. Kaczmarek, F. Karsch, F. Zantow *et al.*, Phys. Rev. D **70**, 074505 (2004) [Erratum: Phys. Rev. D **72**, 059903 (2005)], arXiv: 0406036[hep-lat]
[7] H. Mutuk, Eur. Phys. J. C **81**(4), 367 (2021), arXiv: 2104.11823[hep-ph]
[8] P. Gubler, T. Song, and S. H. Lee, Phys. Rev. D **101**(11), 114029 (2020), arXiv: 2003.09073[hep-ph]
[9] R. F. Lebed, R. E. Mitchell, and E. S. Swanson, Prog. Part. Nucl. Phys. **93**, 143 (2017), arXiv: 1610.04528[hep-ph]
[10] M. N. Sergeenko, Eur. Phys. J. C **72**, 2128 (2012), arXiv: 1206.7099[hep-ph]
[11] M. Baker, J. S. Ball, and F. Zachariasen, Phys. Rev. D **56**, 4400 (1997), arXiv: 9705207[hep-ph]
[12] G. S. Bali, Phys. Rept. **343**, 1 (2001), arXiv: hep-ph/0001312[hep-ph]
[13] C. Ratti, M. A. Thaler, and W. Weise, Phys. Rev. D **73**, 014019 (2006), arXiv: hep-ph/0506234[hep-ph]
[14] M. Lüscher, JHEP **08**, 071 (2010) [Erratum: JHEP **03**, 092 (2014)], arXiv: 1006.4518[hep-lat]
[15] Y. Koma and M. Koma, Phys. Rev. D **95**(9), 094513 (2017), arXiv: 1703.06247[hep-lat]
[16] N. Brambilla, V. Leino, O. Philipsen *et al.*, Phys. Rev. D **105**(5), 054514 (2022), arXiv: 2106.01794[hep-lat]
[17] C. Schlosser and M. Wagner, Phys. Rev. D **105**(5), 054503 (2022), arXiv: 2111.00741[hep-lat]
[18] P. Bicudo, M. Cardoso, and O. Oliveira, Phys. Rev. D **77**, 091504 (2008), arXiv: 0704.2156[hep-lat]
[19] A. K. Rai, B. Patel, and P. C. Vinodkumar, Phys. Rev. C **78**, 055202 (2008), arXiv: 0810.1832[hep-ph]
[20] S. Fleming and T. Mehen, Phys. Rev. D **73**, 034502 (2006), arXiv: 0509313[hep-ph]
[21] Z. B. Kang, Y. Q. Ma, and R. Venugopalan, JHEP **01**, 056 (2014), arXiv: 1309.7337[hep-ph]
[22] P. Sun, C. P. Yuan, and F. Yuan, Phys. Rev. D **88**, 054008 (2013), arXiv: 1210.3432[hep-ph]
[23] B. A. Kniehl, A. A. Penin, V. A. Smirnov *et al.*, Nucl. Phys. B **635**, 357 (2002), arXiv: 0203166[hep-ph]
[24] H. B. Meyer, Eur. Phys. J. A **47**, 86 (2011), arXiv: 1104.3708[hep-lat]
[25] J. M. Maldacena, Adv. Theor. Math. Phys. **2**, 231 (1998), arXiv: 9711200[hep-th]
[26] E. Witten, Adv. Theor. Math. Phys. **2**, 253 (1998), arXiv: 9802150[hep-th]
[27] S. S. Gubser, I. R. Klebanov, and A. M. Polyakov, Phys. Lett. B **428**, 105 (1998), arXiv: 9802109[hep-th]
[28] O. Aharony, S. S. Gubser, J. M. Maldacena *et al.*, Phys. Rept. **323**, 183 (2000), arXiv: 9905111[hep-th]
[29] E. Witten, Adv. Theor. Math. Phys. **2**, 505 (1998), arXiv: 9803131[hep-th]
[30] J. M. Maldacena, Phys. Rev. Lett. **80**, 4859 (1998), arXiv: 9803002[hep-th]
[31] J. Zhou, X. Chen, Y. Q. Zhao *et al.*, Phys. Rev. D **102**(8), 086020 (2020), arXiv: 2006.09062[hep-ph]
[32] J. Zhou, X. Chen, Y. Q. Zhao *et al.*, Phys. Rev. D **102**(12), 126029 (2021)

[33] O. Kaczmarek, F. Karsch, P. Petreczky *et al*., Phys. Lett. B **543**, 41 (2002), arXiv: 0207002[hep-lat]
[34] V. Forini, JHEP **11**, 079 (2010), arXiv: 1009.3939[hep-th]
[35] S. Nojiri and S. D. Odintsov, Phys. Lett. B **458**, 226 (1999), arXiv: 9904036[hep-th]
[36] I. Aref'eva and K. Rannu, JHEP **05**, 206 (2018), arXiv: 1802.05652[hep-th]
[37] L. Barosi, F. A. Brito, and A. R. Queiroz, JHEP **04**, 030 (2009), arXiv: 0812.4841[hep-th]
[38] C. Ewerz, O. Kaczmarek, and A. Samberg, JHEP **03**, 088 (2018), arXiv: 1605.07181[hep-th]
[39] A. Rothkopf, Phys. Rept. **858**, 1 (2020), arXiv: 1912.02253[hep-ph]
[40] H. Bohra, D. Dudal, A. Hajilou *et al*., Phys. Lett. B **801**, 135184 (2020), arXiv: 1907.01852[hep-th]
[41] D. Dudal and S. Mahapatra, Phys. Rev. D **96**(12), 126010 (2017), arXiv: 1708.06995[hep-th]
[42] J. Zhou, S. Zhang, J. Chen *et al*., Phys. Lett. B **844**, 138116 (2023), arXiv: 2310.15609[hep-ph]
[43] J. Zhou and X. Leng, Phys. Rev. D **110**(7), 074003 (2024)
[44] D. Bala *et al*. (HotQCD), Phys. Rev. D **105**(5), 054513 (2022), arXiv: 2110.11659[hep-lat]
[45] N. Brambilla, M. Á. Escobedo, A. Islam *et al*., JHEP **08**, 303 (2022), arXiv: 2205.10289[hep-ph]
[46] L. Thakur, N. Haque, and Y. Hirono, JHEP **06**, 071 (2020), arXiv: 2004.03426[hep-ph]
[47] Y. Kinar, E. Schreiber, and J. Sonnenschein, Nucl. Phys. B **566**, 103 (2000), arXiv: 9811192[hep-th]
[48] H. Boschi-Filho, N. R. F. Braga, and C. N. Ferreira, Phys. Rev. D **73**, 106006 (2006) [Erratum: Phys. Rev. D **74**, 089903 (2006)], arXiv: 0512295[hep-th]
[49] H. Boschi-Filho, N. R. F. Braga, and C. N. Ferreira, Phys. Rev. D **74**, 086001 (2006), arXiv: 0607038[hep-th]
[50] C. A. Meyer and E. S. Swanson, Prog. Part. Nucl. Phys. **82**, 21 (2015), arXiv: 1502.07276[hep-ph]
[51] C. McNeile *et al*. (UKQCD), Phys. Rev. D **65**, 094505 (2002), arXiv: 0201006[hep-lat]
[52] P. Lacock *et al*. (UKQCD), Phys. Lett. B **401**, 308 (1997), arXiv: 9611011[hep-lat]
[53] B. Barsbay, K. Azizi, and H. Sundu, Phys. Rev. D **109**(9), 094034 (2024), arXiv: 2402.19006[hep-ph]
[54] E. Klempt and A. Zaitsev, Phys. Rept. **454**, 1 (2007), arXiv: 0708.4016[hep-ph]
[55] F. E. Close and S. Godfrey, Phys. Lett. B **574**, 210 (2003), arXiv: 0305285[hep-ph]
[56] M. Takizawa and S. Takeuchi, PTEP **2013**, 093D01 (2013), arXiv: 1206.4877[hep-ph]
[57] H. X. Chen, W. Chen, X. Liu *et al*., Rept. Prog. Phys. **86**(2), 026201 (2023), arXiv: 2204.02649[hep-ph]
[58] I. J. General, S. R. Cotanch, and F. J. Llanes-Estrada, Eur. Phys. J. C **51**, 347 (2007), arXiv: 0609115[hep-ph]
[59] J. J. Dudek and R. G. Edwards, Phys. Rev. D **85**, 054016 (2012), arXiv: 1201.2349[hep-ph]
[60] A. Esposito, A. Pilloni, and A. D. Polosa, Phys. Lett. B **758**, 292 (2016), arXiv: 1603.07667[hep-ph]
[61] F. J. Llanes-Estrada and S. R. Cotanch, Phys. Lett. B **504**, 15 (2001), arXiv: 0008337[hep-ph]
[62] J. M. Richard, Few Body Syst. **57**(12), 1185 (2016), arXiv: 1606.08593[hep-ph]
[63] N. Brambilla, W. K. Lai, J. Segovia *et al*., Phys. Rev. D **101**(5), 054040 (2020), arXiv: 1908.11699[hep-ph]
[64] O. Andreev and V. I. Zakharov, Phys. Lett. B **645**, 437 (2007), arXiv: 0607026[hep-ph]
[65] O. Andreev, Phys. Rev. D **86**, 065013 (2012), arXiv: 1207.1892[hep-ph]
[66] J. J. Jiang, Y. Z. Xiao, J. Qin *et al*., Chin. Phys. C **47**(1), 013106 (2023), arXiv: 2212.03541[hep-ph]
[67] O. Andreev, Phys. Rev. D **87**(6), 065006 (2013), arXiv: 1211.0930[hep-ph]
[68] J. Zhou and M. Zhu, *Hybrid Meson Pseudopotentials from a Holographic Model with Gluon Condensation*, Eur. Phys. J. C (2026), in press
[69] D. Mateos and D. Trancanelli, Phys. Rev. Lett. **107**, 101601 (2011), arXiv: 1105.3472[hep-th]
[70] D. Mateos and D. Trancanelli, JHEP **07**, 054 (2011), arXiv: 1106.1637[hep-th]
[71] J. Zhou, K. Bitaghsir Fadafan, and X. Chen, Eur. Phys. J. C **84**(7), 762 (2024), arXiv: 2403.07330[hep-ph]
[72] K. Bitaghsir Fadafan, D. Giataganas, and H. Soltanpanahi, JHEP **11**, 107 (2013), arXiv: 1306.2929[hep-th]
[73] L. Zhang, F. Y. Cai, and X. Chen, Chin. Phys. C **49**(1), 013112 (2025), arXiv: 2410.05691[hep-ph]
[74] O. Andreev, Phys. Rev. D **93**(10), 105014 (2016), arXiv: 1511.03484[hep-ph]
[75] P. Cheng, Q. Meng, Q. Wu *et al*., Phys. Rev. D **98**(11), 116010 (2018), arXiv: 1802.01119[hep-ph]